
This is an electronic reprint of the original article.
This reprint may differ from the original in pagination and typographic detail.

Zhang, Jianxin; Said, Arshe; Han, Bing; Louhi-Kultanen, Marjatta
Semi-batch evaporative crystallization and drying of cobalt sulphate hydrates

Published in:
Hydrometallurgy

DOI:
[10.1016/j.hydromet.2022.105821](https://doi.org/10.1016/j.hydromet.2022.105821)

Published: 01/02/2022

Document Version
Publisher's PDF, also known as Version of record

Published under the following license:
CC BY

Please cite the original version:
Zhang, J., Said, A., Han, B., & Louhi-Kultanen, M. (2022). Semi-batch evaporative crystallization and drying of cobalt sulphate hydrates. *Hydrometallurgy*, 208, Article 105821. <https://doi.org/10.1016/j.hydromet.2022.105821>

This material is protected by copyright and other intellectual property rights, and duplication or sale of all or part of any of the repository collections is not permitted, except that material may be duplicated by you for your research use or educational purposes in electronic or print form. You must obtain permission for any other use. Electronic or print copies may not be offered, whether for sale or otherwise to anyone who is not an authorised user.



Semi-batch evaporative crystallization and drying of cobalt sulphate hydrates

Jianxin Zhang, Arshe Said, Bing Han, Marjatta Louhi-Kultanen*

Department of Chemical and Metallurgical Engineering, School of Chemical Engineering, Aalto University, P.O. Box 16100, 00076 Aalto (Espoo), Finland

ARTICLE INFO

Keywords:

Cobalt sulfate
Hydrates
Evaporative crystallization
Drying
Dehydration

ABSTRACT

Semi-batch evaporative crystallization of CoSO_4 was investigated at various underpressures and with different heating powers. The underpressures for boiling aqueous CoSO_4 solutions at various temperatures and concentrations were measured and compared to predicted values obtained by the Aspen Plus Version 11 process simulation software. The presence of CoSO_4 solute decreased the underpressure for boiling solution in comparison to pure water. In the evaporative crystallization experiments, CoSO_4 crystallized as $\text{CoSO}_4 \cdot 7\text{H}_2\text{O}$ at evaporation temperatures of 30 °C and 40 °C, whereas $\text{CoSO}_4 \cdot 6\text{H}_2\text{O}$ crystallized at 60 °C and 80 °C. The crystals obtained at 30 °C and 40 °C were mainly agglomerates of octahedron shaped particles. Heating power and mixing speed had significant effects on the evaporation flux and particle size distribution of the products. Smaller crystals were produced with higher heating power and higher mixing speed due to the enhancement of evaporation. Dehydration of the formed cobalt sulfate heptahydrate in the drying process was also investigated with two variables: drying temperature and drying time. The crystallization at 40 °C yielded unstable $\text{CoSO}_4 \cdot 7\text{H}_2\text{O}$, which tended to dehydrate in a temperature range between 23 °C and 60 °C; these crystals were used in the study of crystal drying. At a drying temperature of 23 °C, $\text{CoSO}_4 \cdot 7\text{H}_2\text{O}$ transferred and stabilized as $\text{CoSO}_4 \cdot 6\text{H}_2\text{O}$. At drying temperatures of 40 °C and 60 °C, the stable hydrate form was $\text{CoSO}_4 \cdot \text{H}_2\text{O}$. Gravimetric analysis, crystal habit, XRD, and Raman analyses were successfully utilized for the investigation of the transformation of the hydrate form during drying.

1. Introduction

Cobalt sulfate, which commonly exists as cobalt sulfate heptahydrate ($\text{CoSO}_4 \cdot 7\text{H}_2\text{O}$), is one of the most important cobalt salts. It is widely used in electrochemical materials, ceramic applications, and even in the agricultural sector. Nowadays, the use in the rechargeable battery industry has become the most common use for cobalt sulfate, which is applied as a cathode active material. Adding cobalt into the cathode of rechargeable batteries can efficiently improve a battery's life, stability, inhibited corrosion, and performance (Li and Lu, 2020). The demand for cobalt sulfate is continuously rising due to the demand for 5G devices, consumer electronics, and passenger electric vehicles (EVs). Alloy manufacturing is another major application of cobalt sulfate. The addition of cobalt sulfate alloys makes the treated materials much stronger, with higher melting points, superior hot corrosion resistance, and oxidation resistance (Coutsouradis et al., 1987; Sato et al., 2006).

Cobalt sulfate is also employed as a pigment in the porcelain and glass industries and as a coloring agent in ceramics, enamels, and glazes to prevent discoloration (Yang et al., 2002). In the farming sector, cobalt sulfate has been used as an additive in soils and animal feeds to supply trace minerals (Suslick, 1998). According to an EU report (European Commission, 2020), cobalt has already been identified as a critical material in the EU.

Cobalt sulfate is a water-soluble divalent cobalt(II) salt. The generation and purification of cobalt sulfate solution have attracted a lot of interest, especially in the battery recovery industry (Devi et al., 1998; Huang et al., 2019; Petranikova et al., 2019; Reddy et al., 2009; Swain et al., 2007). Vielma (2021) modelled thermodynamics of aqueous CoSO_4 solutions and various hydrates in temperature range between 270 K and 374 K. However, the studies on cobalt sulfate crystallization from aqueous solution are limited. Aktas et al. (2013) investigated cobalt sulfate precipitation by anti-solvent crystallization with ethanol and

Abbreviations: PSD, particle size distribution; SEM, Scanning Electron Microscopy; TG-DTA, Thermogravimetry and Differential Thermal Analysis; ΔT , Temperature difference between heating jacket and solution; XRD, X-ray Powder Diffraction.

* Corresponding author.

E-mail address: marjatta.louhi-kultanen@aalto.fi (M. Louhi-Kultanen).

<https://doi.org/10.1016/j.hydromet.2022.105821>

Received 30 June 2021; Received in revised form 11 January 2022; Accepted 15 January 2022

Available online 19 January 2022

0304-386X/© 2022 The Authors. Published by Elsevier B.V. This is an open access article under the CC BY license (<http://creativecommons.org/licenses/by/4.0/>).

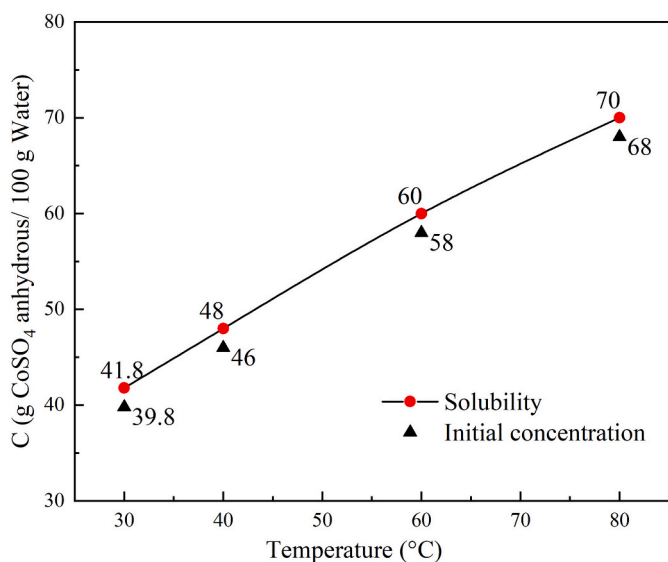


Fig. 1. Solubility data for cobalt sulfate and initial solution concentration at different temperatures.

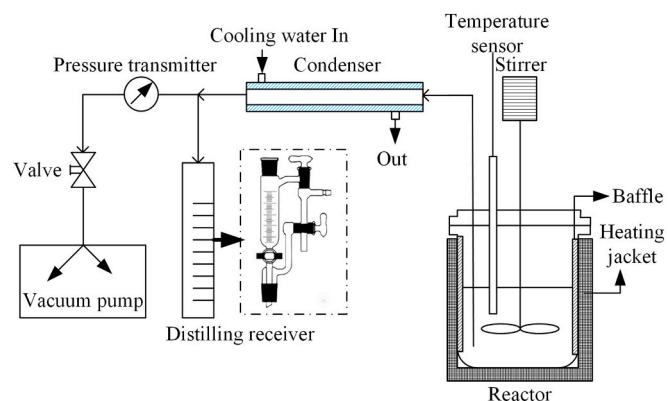


Fig. 2. Experimental setup diagram of semi-batch evaporative crystallization.

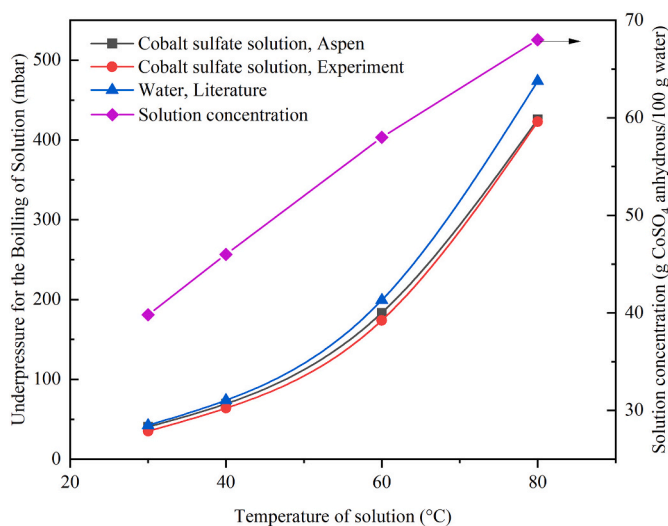


Fig. 3. Underpressure at boiling point of saturated cobalt sulfate solutions and water.

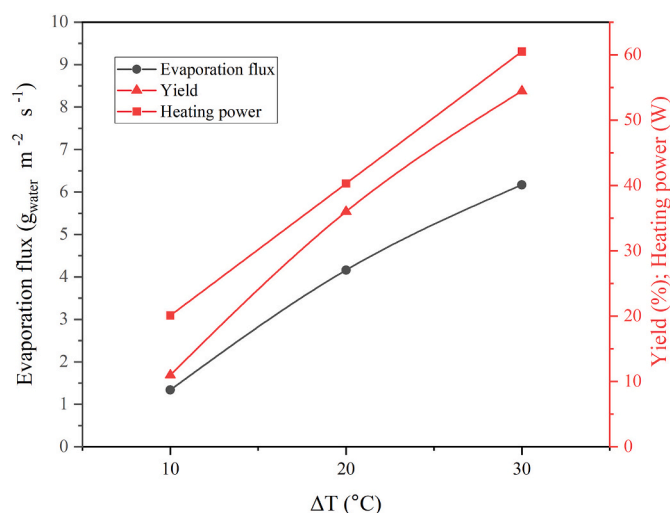


Fig. 4. Evaporation fluxes, heating power and product yields at different ΔT at 40 °C, mixing speed of 650 rpm, and evaporation time of 30 min.

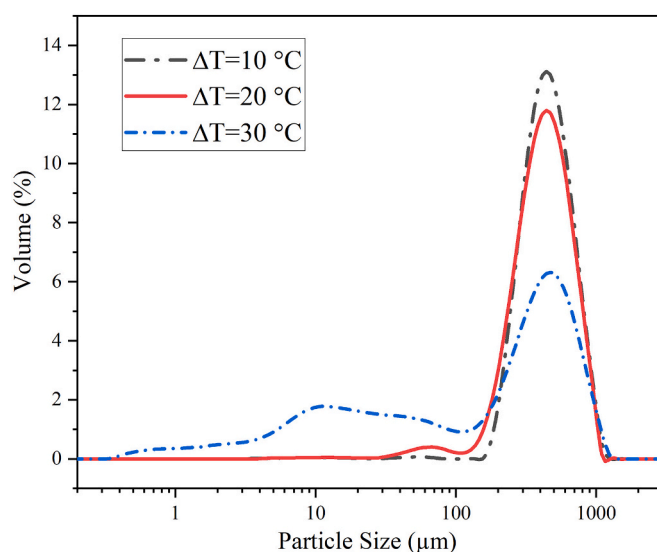


Fig. 5. PSD analyses of cobalt sulfate obtained at different ΔT values at 40 °C, mixing speed of 650 rpm, and evaporation time of 30 min.

methanol. In their study, a high cobalt sulfate precipitation efficiency was obtained based on the short precipitation times required and good filterability of the obtained $\text{CoSO}_4 \cdot 7\text{H}_2\text{O}$ crystals. This process also had low power consumption as it did not need power for heating or cooling, whereas the consumption of ethanol or methanol was high. The recycling of organic solvents could be a challenge and may make the process less sustainable or energy efficient. In contrast, the crystallization of cobalt sulfate by evaporative crystallization and the evaporation concentrate-cooling crystallization process have been widely applied on industrial scale. In the evaporation process, the solvent is partially separated from solution by consuming a large amount of heat, so that the cobalt sulfate crystallizes out from the solution. However, the process has one major shortcoming: the energy consumption is high due to the high latent heat of evaporation. In the case of water, the latent heat of evaporation is 2260 kJ/kg at ambient pressure and 100 °C. In order to minimize the energy demand in the evaporation process, many technological improvements have been made in recent years, such as multi-effect evaporation and mechanical vapor recompression crystallization (Lu et al., 2017; Said and Louhi-Kultanen, 2019).

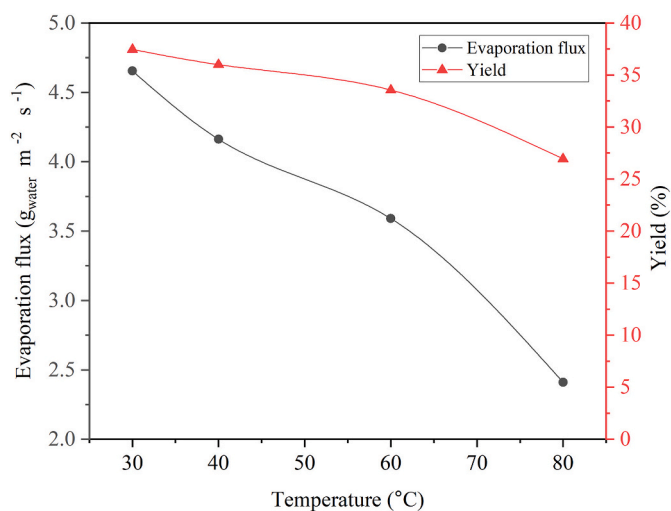


Fig. 6. Evaporation fluxes and product yields at different evaporation temperatures, at a ΔT of 20 °C, evaporation time of 30 min, and mixing speed of 650 rpm.

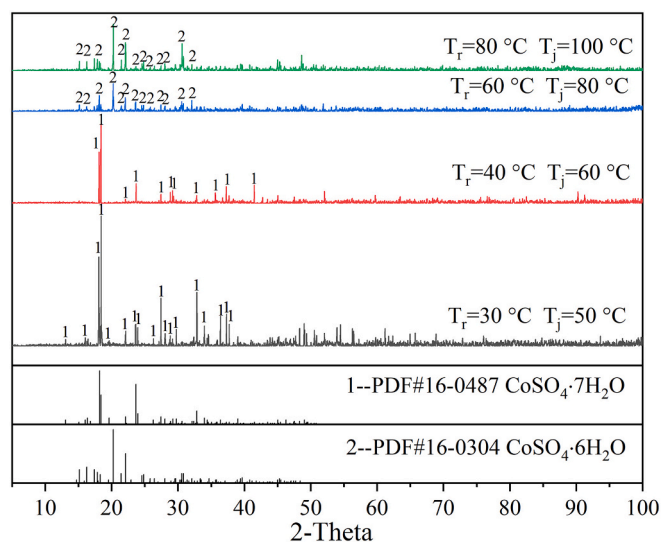


Fig. 7. XRD patterns of crystallized cobalt sulfate hydrates at different evaporation temperatures.

Although evaporative crystallization of cobalt sulfate is widely applied in industrial processes, there are quite few studies reported in literature about the factors affecting the crystal properties and their stability. In the present work, comprehensive studies on evaporative crystallization of cobalt sulfate were carried out with the aim to gain deeper understanding on the influence of operational conditions on crystal properties. The present work focuses on investigating the influences of various factors, including heat energy input, temperature, and mixing, on the evaporation kinetics and crystal properties of cobalt sulfate. In addition, the transformation of the cobalt sulfate hydrate form during drying was studied as well as the changes in drying temperature and drying time.

2. Materials and methods

2.1. Materials

Semi-batch evaporative crystallization was studied with aqueous cobalt sulfate solutions. The synthetic cobalt sulfate solutions were

prepared with analytical grade $\text{CoSO}_4 \cdot 7\text{H}_2\text{O}$ (purity $\geq 99\%$, ACROS ORGANICS) and deionized water. The initial concentration for synthetic cobalt sulfate solution was slightly lower than the solubility of CoSO_4 at different temperatures reported in the literature (Mullin, 2001), as shown in Fig. 1.

2.2. Experimental methods

The experiments were carried out in a 400 ml glass reactor equipped with baffles in an EasyMax 402 stirred tank system (Mettler Toledo). The inside diameter of the reactor was 72.6 mm and the upper surface area of the liquid in the reactor was $A = 4.15 \times 10^{-3} \text{m}^2$. The stirring speed and heating energy were adjusted with iControl software. The solution was mixed by using a pitched-blade turbine with four blades ($\Phi = 38 \text{mm}$). A pressure transmitter (WIKA, A-10, error $< 0.14\%$) and an MPC 301Z vacuum pump (ultimate pressure $< 8 \text{mbar}$, pumping speed 38 l/min) equipped with a valve were used to control the pressure in the crystallizer. A Liebig condenser and distilling receiver (Anschutz-Thiele, straight, 50 ml) was used for vapor condensation and condensate collection. A diagram of the experimental set-up is shown in Fig. 2. In this study, we investigated the effects of crystallization temperature, mixing speed, and heating power on crystal properties. Different evaporation temperatures were controlled by adjusting the pressure to reach the boiling point. Different heating power values were achieved by changing the jacket temperature. The vacuum evaporation step was stopped 30 min after the solution had reached boiling point. After the vacuum evaporation step, the solution temperature was kept constant during an ageing period for another 30 min under atmospheric pressure.

2.3. Characterization

Samples obtained from the crystallization and drying processes were characterized by X-ray powder diffraction (XRD; X'Pert PRO) using a copper radiation source ($\lambda_{\text{K}\alpha 1} = 1.5406 \text{\AA}$) operated at 40kV, with 40mA. The morphology of the products was examined with a scanning electron microscope, (SEM, TESCAN MIRA3). The particle size distribution (PSD) was analyzed with a particle size analyzer (Malvern Master Sizer 2000). Ethanol (99.5%, absolute, VWR) solution was used as the dispersant because of the low solubility of CoSO_4 in ethanol (Stephen and Stephen, 1963). The samples obtained in the various drying processes were also analyzed by using a Raman spectrometer (inVia™ confocal Raman microscope, Renishaw) to verify the hydrate forms. The Thermogravimetry and Differential Thermal Analysis (TG-DTA) measurements were carried with a TA Instruments (TGA Q500) in nitrogen atmosphere in the temperature range between 30 °C and 500 °C at the heating rate of 10 °C/min.

The cobalt sulfate yield percentage in the experiments was calculated using Eq. (1):

$$\text{Yield (\%)} = \frac{m_p}{(m_{i,s} \times w_i)} \times 100 \quad (1)$$

where m_p is the mass of the product (on the basis of anhydrous cobalt sulfate), [g]; $m_{i,s}$ the mass of the initial solution, [g]; and w_i the mass fraction of cobalt sulfate in the initial solution, [g/g initial solution].

The evaporation flux was calculated with Eq. (2):

$$R = \frac{m_{i,s} - m_{e,s}}{t \times S} \quad (2)$$

where R is the evaporation flux of water from the cobalt sulfate solution, [$\text{g}_{\text{water}} \text{m}^{-2} \text{s}^{-1}$]; $m_{e,s}$ the mass of solution weighed after evaporative crystallization, [g]; t the evaporation time initiated when boiling started, [s]; and S the surface area of the upper liquid surface, which in the present work was 0.00415m^2 .

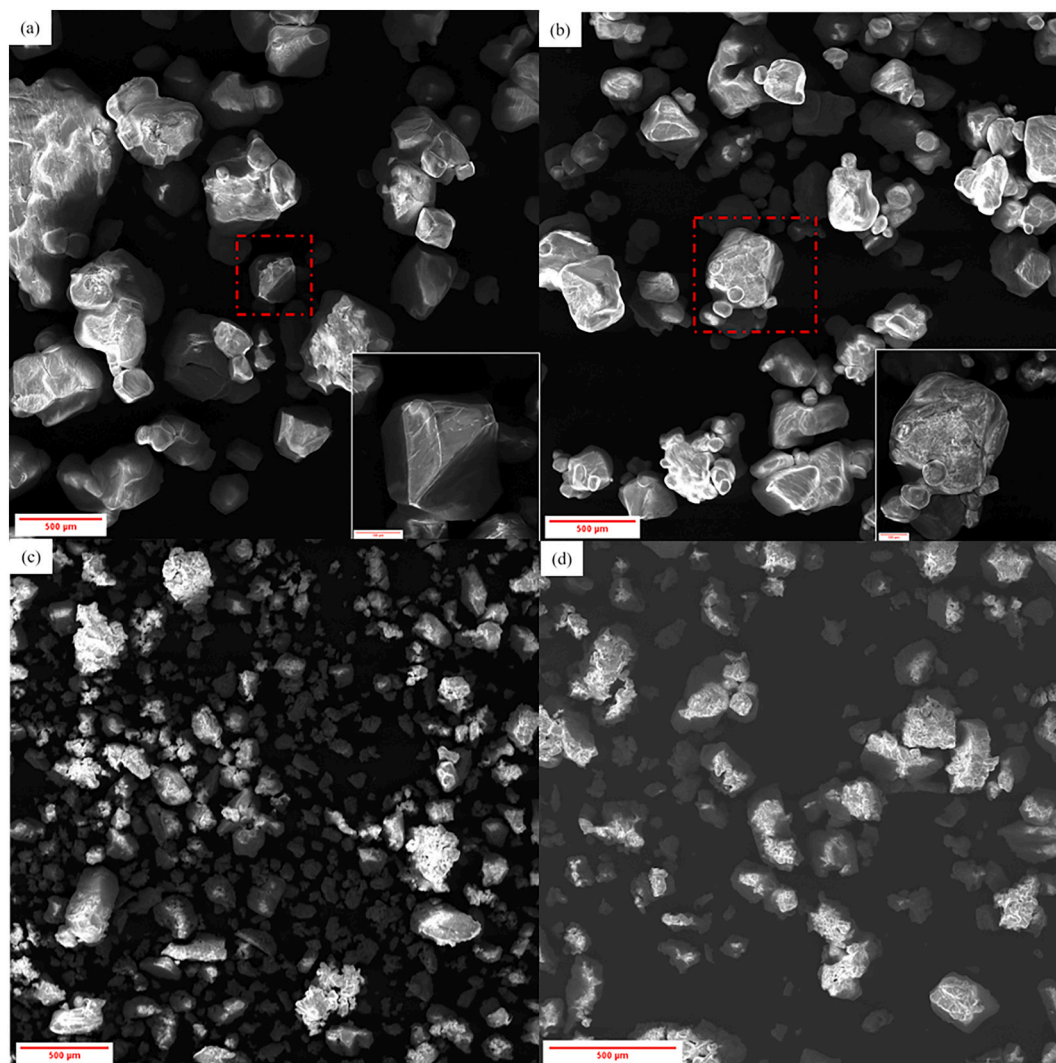


Fig. 8. Characteristic SEM images of crystallized CoSO_4 obtained at different evaporation temperatures: (a) 30 °C, heptahydrate, (b) 40 °C, heptahydrate, (c) 60 °C, hexahydrate, and (d) 80 °C, hexahydrate, with a ΔT of 20 °C, evaporation time of 30 min, and mixing speed of 650 rpm. Scale bar 500 μm .

3. Results and discussion

3.1. Determination of underpressure for evaporative crystallization at selected boiling points

In order to conduct evaporative crystallization experiments at a certain boiling temperature, the operational underpressure had to be adjusted to a certain level with a vacuum pump and sufficient heating power had to be provided to achieve the boiling point. The adjusted underpressures and related boiling points were estimated by Aspen Plus V11 and measured experimentally. The boiling points and saturated vapor pressure of water were taken from the literature (Lide, 2005). The results are shown in Fig. 3. The predicted underpressure for boiling cobalt sulfate solution with various concentration obtained by Aspen Plus V11 were slightly higher than the measured value under the same temperature, but the trends are in good agreement with experimental results. In comparison to the results for water, the dissolved cobalt sulfate decreased the underpressure for boiling the solution. Moreover, the underpressure difference between water and cobalt sulfate solution increased with the increase of concentration.

Based on this result, the operational pressure for vacuum evaporative crystallization at various temperatures can be determined: at 30 °C, 40 °C, 60 °C, and 80 °C, the saturated cobalt sulfate solution boils at 35

mbar, 64 mbar, 174 mbar, and at 423 mbar, respectively.

3.2. Effect of heating power

Beside the crystallization temperature, heating power is one of the principle operational factors affecting the evaporation flux, supersaturation, and product properties. In this study, the variation in heating power was achieved by changing the difference between the temperature of the solution (T_s) and the heating jacket (T_j). Here, we set the temperature difference (ΔT) to 10, 20, and 30 °C. The other conditions were as follows: evaporation temperature of 40 °C, pressure of 64 mbar (abs), initial solution of 46 g anhydrous $\text{CoSO}_4/100$ g water, evaporation time of 30 min, and mixing speed of 650 rpm (tip speed of 1.29 m/s).

The evaporation fluxes and product yields obtained at different heating powers are illustrated in Fig. 4. The evaporation flux and product yields showed a significant increase with the increase in ΔT . The larger ΔT gave a higher heating power and thus led to higher evaporation fluxes. As expected, a higher yield was obtained at a higher ΔT . When the ΔT was 30 °C, over 55% cobalt sulfate was crystallized after evaporation for 30 min, although only about 35% water was evaporated. The reason is that the cobalt sulfate crystallized in hydrate form and therefore, water was transferred from the solution to hydrate crystals. The particle size distribution (PSD) analysis results for products

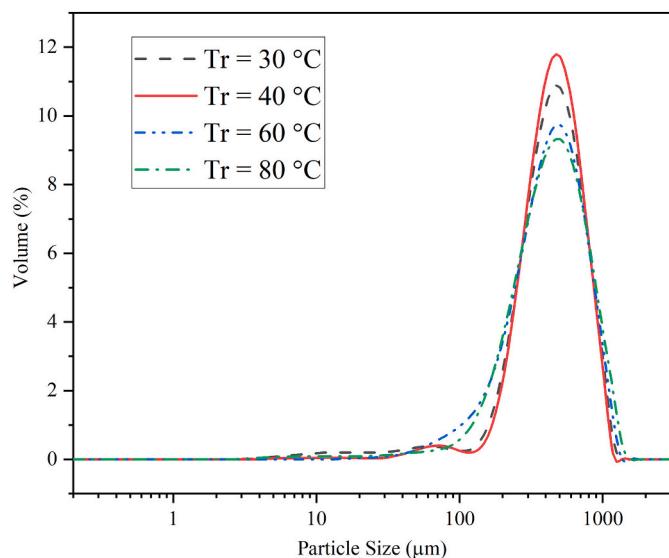


Fig. 9. Particle size distribution of cobalt sulfate obtained at different evaporation temperatures, a ΔT of 20 °C, evaporation time of 30 min, and mixing speed of 650 rpm.

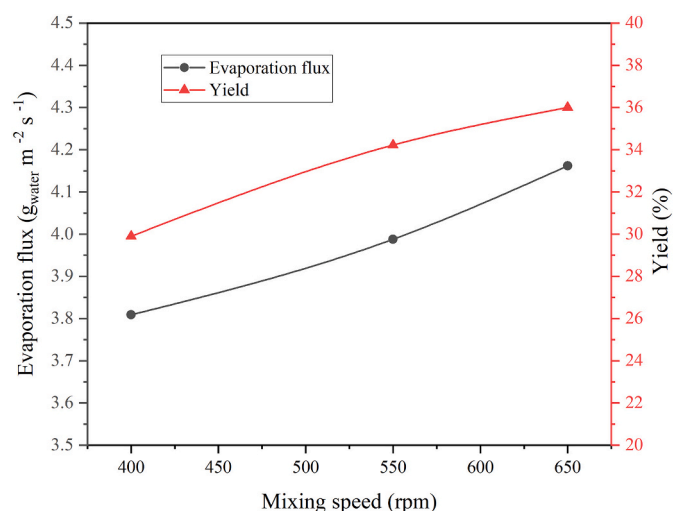


Fig. 10. Evaporation flux and product yields at different mixing speeds at a temperature of 40 °C, ΔT of 20 °C, and evaporation time of 30 min.

obtained with different ΔT values are shown in Fig. 5, which depicts that the product obtained at a high ΔT is smaller than that obtained from a low ΔT . The mean particle size for a ΔT of 10, 20, and 30 °C was 509, 480, and 310 μm , respectively. Moreover, the product obtained at low heating power had a narrower size distribution compared to the products obtained with higher heating power. The higher evaporation flux provides a higher supersaturation degree which can increase both the crystal growth rate and nucleation rate. If nucleation dominates crystallization, the ratio of smaller crystals in the crystalline product becomes larger.

The heat energy input at different ΔT was calculated based on the heat transfer between the jacket and solution in the vacuum evaporation process, following Eq. (3). The heat energy input was 36.3, 72.7, and 109 kJ with a heating power of 20.1, 40.3, and 60.5 W for a ΔT of 10, 20, and 30 °C, respectively.

$$Q = q \times t = U \times A \times \Delta T \times t \quad (3)$$

where Q is the heat energy input, [J]; q the heating power, [W]; U the

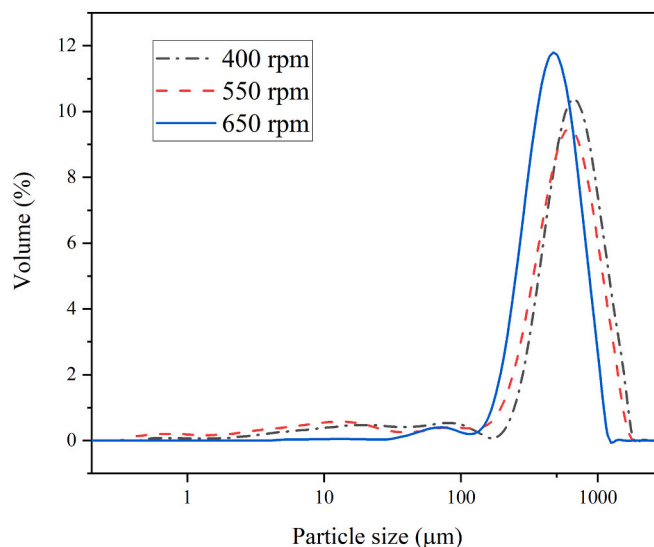


Fig. 11. Particle size distribution of cobalt sulfate obtained with various mixing speeds at a temperature of 40 °C, ΔT of 20 °C, and evaporation time of 30 min.

overall transfer coefficient (in the present work $U = 243.3 \text{ W}/(\text{m}^2 \text{ } ^\circ\text{C})$, which was measured by calorimetry built in the EasyMax system with a mixing speed of 650 rpm and solution temperature of 40 °C); A is the heat transfer surface area, in the present work $A = 8.3 \times 10^{-3} \text{ m}^2$; ΔT the temperature difference between jacket and solution, [°C]; and t the time needed for evaporation, $t = 1800 \text{ s}$.

3.3. Effect of evaporation temperature

In the evaporative crystallization process, it is evident that temperature is one of the key factors affecting the energy consumption and product properties. In the crystallization of cobalt sulfate, temperature affects the hydrate form of the products, which was investigated more comprehensively in the present work. In this study, four temperatures of 30, 40, 60, and 80 °C were selected. The operating pressure was varied by changing the evaporation temperature based on the determination of vapor pressure for different boiling temperatures; namely, 35 mbar for 30 °C, 64 mbar for 40 °C, 174 mbar for 60 °C, and 423 mbar for 80 °C. The other conditions were as follows: ΔT (heating power) of 20 °C, evaporation time of 30 min, and mixing speed of 650 rpm. The initial solution concentrations of 39.8, 46, 58, and 68 g anhydrous $\text{CoSO}_4/100 \text{ g}$ water were used in the experiments carried out at temperatures of 30, 40, 60, and 80 °C, respectively.

As shown in Fig. 6, the evaporation fluxes decrease significantly with an increase in temperature. More water evaporated at lower temperature, 34.7 g at 30 °C and 18 g at 80 °C, whereas the product yields were 37.4% at 30 °C and 27% at 80 °C, respectively. It seems that the hydrate formation starts to affect here: evaporation of more water at 30 °C, along with higher degree of hydration leads to greater product yield. On the other hand, it is expected that more cobalt sulfate crystallizes from solutions of higher initial concentration at higher temperature, corresponding to the same amount of water evaporated. The XRD patterns for products obtained at different temperatures are shown in Fig. 7. It can be seen in Fig. 7 that cobalt sulfate crystallized as heptahydrate at 30 °C and 40 °C and hexahydrate at 60 °C and 80 °C. Based on the thermodynamics studies of Vielma (2021), cobalt sulfate should crystallize as cobalt sulfate monohydrate at 80 °C. The reason we obtained hexahydrate at 80 °C is probably because of relatively high overall crystallization rate. The SEM images of solid crystals produced at various temperatures are presented in Fig. 8. The crystals formed at 30 °C and 40 °C had a similar morphology of octahedron crystal shape, and agglomerates were formed during the process. By contrast, the product



Fig. 12. Sample images with different drying times at various drying temperatures.

crystallized at 60 °C and 80 °C did not have a uniform shape and the agglomeration tendency was higher than that at the lower temperature. The mother liquor with a higher concentration at higher temperature could promote the agglomeration due to higher degree of supersaturation. The PSD of products crystallized at different temperatures is illustrated in Fig. 9. It shows that the crystals obtained at 60 °C and 80 °C had a broader size distribution compared to the crystals obtained at 30 °C and 40 °C, which agrees well with the SEM analyses. The average particle size of products obtained at different temperatures were very similar, with 470, 480, 466, and 481 μm for 30, 40, 60, and 80 °C, respectively.

3.4. Effect of mixing

Mixing has a significant effect on the crystallization process. For the evaporative crystallization process, mixing will affect the heat transfer in solution, evaporation flux, and further product properties. In this work, three different mixing speeds for cobalt sulfate crystallization were investigated, namely 400, 550, and 650 rpm with corresponding tip speeds of 0.79 m/s, 1.09 m/s, and 1.29 m/s, respectively. The other crystallization conditions were as follows: evaporation temperature of 40 °C, ΔT of 20 °C, initial solution of 46 g anhydrous CoSO_4 /100 g water, evaporation time of 30 min, and pressure of 64 mbar.

The evaporation flux and product yields at different mixing speeds are presented in Fig. 10. The evaporation flux and product yields increased gradually with a rise in mixing speed from 400 to 650 rpm, which means that a higher mixing rate enhances the heat transfer in the solution, thus promoting evaporation and solid crystallization. The overall heat transfer coefficient at different mixing speeds was measured by calorimetry. The results were 205.5, 227.1, and 243.3 $\text{W}/(\text{m}^2 \text{ } ^\circ\text{C})$, at mixing speeds of 400, 550, and 650 rpm, respectively. The results showed that heat transfer was enhanced by increasing mixing intensity when the ΔT was the same. The particle size was smaller when the mixing speed was higher, as can be seen in Fig. 11. This is because a higher mixing speed promotes evaporation, which increases the degree of supersaturation. In turn, higher supersaturation enhances nucleation, resulting in the formation of small particles. Moreover, the higher mixing speed can enhance the diffusion of the solute in the solution and the supersaturation and therefore, the driving force, supersaturation degree, usually becomes more uniform in the crystallizer. The crystals obtained at higher mixing speed are more uniform based on PSD results,

as shown in Fig. 11.

3.5. Dehydration studies

The crystalline products obtained proved to be unstable, which could be seen from the dehydration occurring during the drying of the crystals. The heptahydrate products were able to transform into hexahydrate or even monohydrate at a certain temperature and drying time (Rakuzin and Brodski, 1927). To investigate the dehydration of the cobalt sulfate heptahydrate obtained during the drying process, we carried out a comprehensive study with the samples obtained with an evaporation temperature of 40 °C, ΔT of 20 °C, mixing speed of 650 rpm, at different drying temperatures and times. The drying experiments were carried out with a ventilated oven at temperatures of 23 °C, 40 °C, and 60 °C. The samples were collected after the drying times of 8, 24, 48, and 168 h.

The images of samples in different drying conditions are displayed in Fig. 12. The color of the samples varied clearly over time. At a drying temperature of 23 °C, the color of the sample changed from red to pink after 168 h of drying. The pink particles already appeared after 24 h drying at 23 °C. The weight loss curves in Fig. 13(a) and XRD patterns in Fig. 13(b) show that the weight losses showed a significant increase during the drying time from 8 h to 24 h; however, after 48 h the weight remained stable. The XRD patterns for samples obtained at different drying times also showed the transformation of hydrate with the appearance of diffraction peaks for $\text{CoSO}_4 \cdot 6\text{H}_2\text{O}$ occurring after 24 h of drying. However, the diffraction peaks for $\text{CoSO}_4 \cdot 7\text{H}_2\text{O}$ disappeared when the samples were dried at 23 °C over 48 h, showing that the transformation from heptahydrate to hexahydrate started to occur after crystals had dried for 24 h. Dehydration was completed when the crystals had dried for 48 h. It is pointed out here that $\text{CoSO}_4 \cdot 6\text{H}_2\text{O}$ crystals did not dehydrate during 168 h at 23 °C.

As the drying temperature increased, the final hydrate form and dehydration kinetics changed. In Fig. 13(a) and (c), it can be seen that the original sample transformed from heptahydrate into hexahydrate very rapidly and almost ended after 8 h of drying when the samples were dried at 40 °C. The weight loss changed slightly between 8 h and 24 h. Cobalt sulfate hexahydrate was still the main phase in the sample obtained after 24 h drying at 40 °C, which was verified by XRD analyses. After 48 h of drying, the weight loss had increased significantly during this period. This is because the sample dehydrated from hexahydrate to monohydrate. The sample dried after 48 h had some reddish particles, as

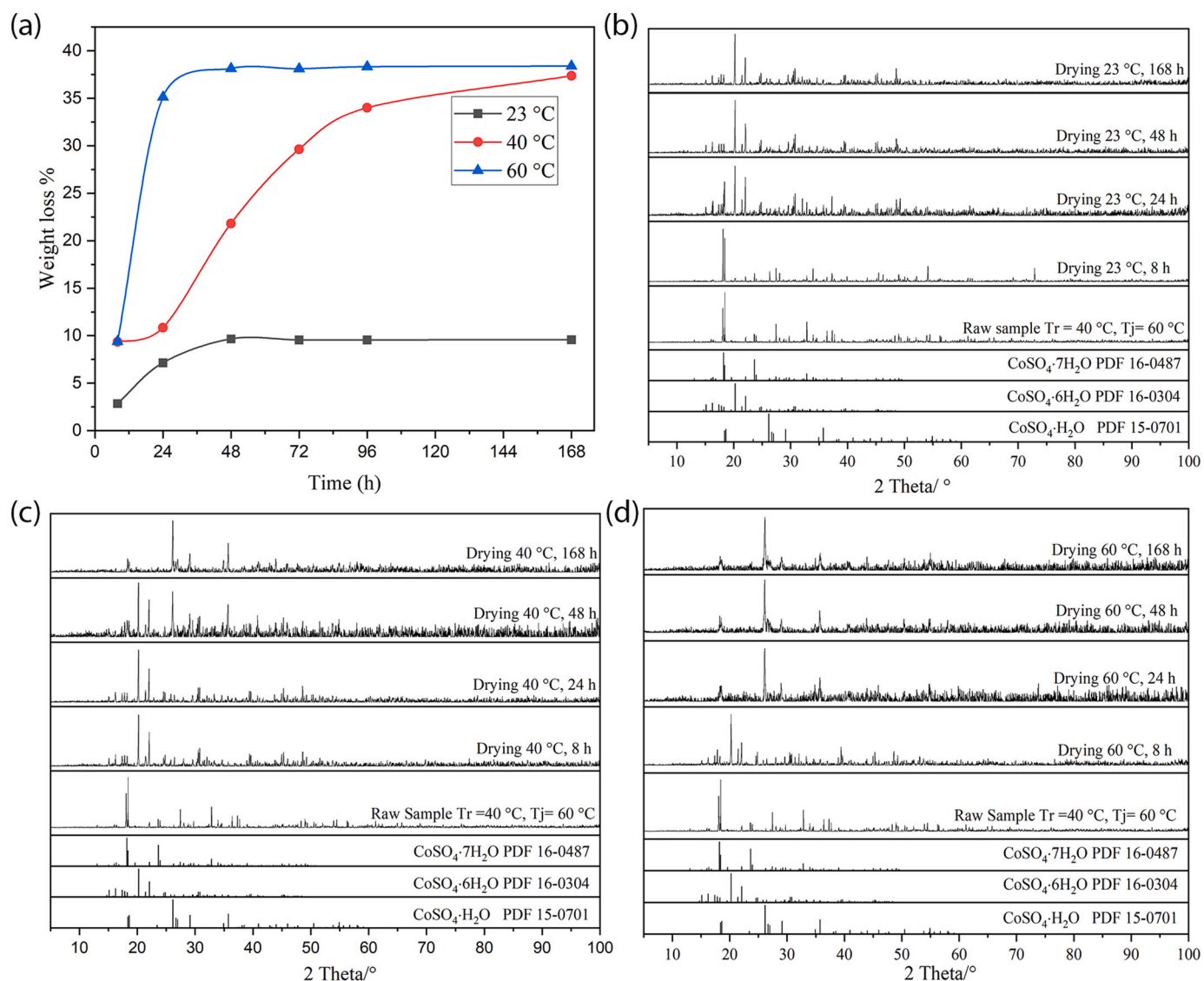


Fig. 13. Drying of crystals: (a) weight loss during drying process: XRD patterns for samples dried for various times at temperatures of (b) 23 °C; (c) 40 °C; (d) 60 °C.

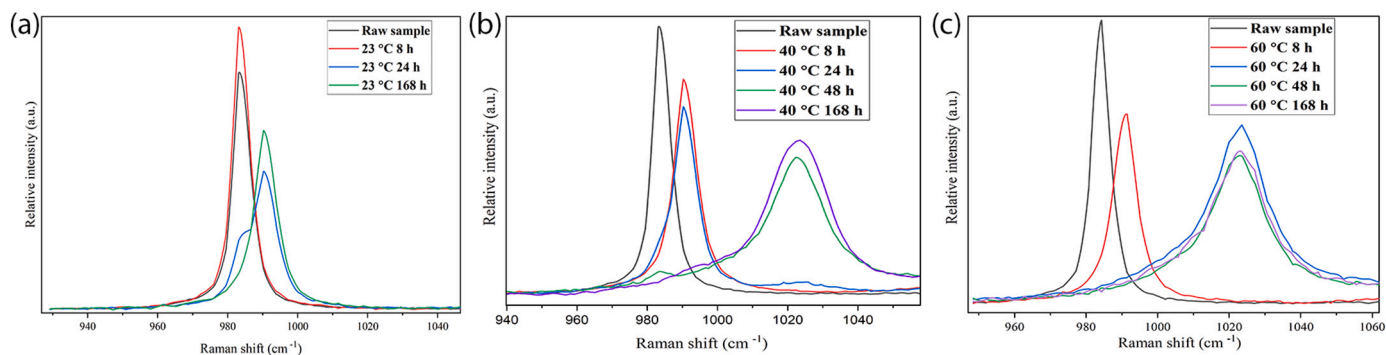


Fig. 14. Selected Raman spectra for ν₁ (SO₄) mode for samples with different drying times at temperatures of (a) 23 °C; (b) 40 °C; (c) and 60 °C.

shown in Fig. 12. The XRD analysis showed that monohydrate crystals had formed. Then the sample completely transformed into monohydrate form with a reddish color after continuous drying for 168 h. The results of the XRD patterns only show the diffraction peaks of CoSO₄·H₂O. The total weight loss was 38%, which is close to the theoretical weight loss of 38.4% for the dehydration of CoSO₄·7H₂O to CoSO₄·H₂O.

At a drying temperature of 60 °C, the dehydration took place even faster. In Fig. 13(a), it is shown that the weight losses increased significantly after 8 h and 24 h of drying and the weights were constant after drying for 48 h. The XRD patterns in Fig. 13(d) also illustrate the dehydration of the sample in the drying process: CoSO₄·7H₂O (Original)- CoSO₄·6H₂O (8 h)- CoSO₄·H₂O (24–168 h), showing good

agreement with the sample's color, which changed from red to pink and then reddish. The TG-DTA analysis was carried out for the $\text{CoSO}_4 \cdot 7\text{H}_2\text{O}$ sample and the results are shown in Fig. S.1. Four dehydration steps occurring at temperatures of 101, 112, 246, and 295 °C can be seen in Fig. S.1. The total weight loss was 41.4%, which is lower than the theoretical weight loss of 44.8% for $\text{CoSO}_4 \cdot 7\text{H}_2\text{O}$. This is probably caused by the dehydration of $\text{CoSO}_4 \cdot 7\text{H}_2\text{O}$ at a temperature lower than 30 °C, where the data was not collected. Compared to the results reported by Sinha et al. (1989) and Nandi and Kher (1980), the crystallized $\text{CoSO}_4 \cdot 7\text{H}_2\text{O}$ in this study seems to be less stable than the samples obtained by slow evaporative crystallization in their study. The dehydration temperatures differed as well. According to Sinha et al., $\text{CoSO}_4 \cdot 7\text{H}_2\text{O}$ dehydrated firstly to $\text{CoSO}_4 \cdot 6\text{H}_2\text{O}$ at around 120 °C. At higher temperatures of 162 °C and 185 °C, $\text{CoSO}_4 \cdot 6\text{H}_2\text{O}$ transferred firstly to $\text{CoSO}_4 \cdot 3\text{H}_2\text{O}$ and then $\text{CoSO}_4 \cdot \text{H}_2\text{O}$. The dehydration of $\text{CoSO}_4 \cdot \text{H}_2\text{O}$ occurred approximately at 295 °C.

The Raman analysis results for samples obtained from different drying process times are shown in Figs. S.2–S.4 in supplementary materials. The vibrational wavenumber of the ν_1 (SO_4) mode (symmetric stretching vibration of the SO_4^{2-} ion) could be useful for analyzing the strength of the S—O bond and the chemistry surrounding the SO_4^{2-} ion (Chio et al., 2007). In the crystallographic arrangement of cobalt sulfate hydrates (Elerman, 1988; Giester and Wildner, 1991; Redhammer et al., 2007), the SO_4^{2-} ion in $\text{CoSO}_4 \cdot 6\text{H}_2\text{O}$ and $\text{CoSO}_4 \cdot 7\text{H}_2\text{O}$ has a similar chemical environment, forming complex H-bonding within a lattice and coordinated H_2O but is less extensive. In comparison, the SO_4^{2-} ion in $\text{CoSO}_4 \cdot \text{H}_2\text{O}$ also forms a H-bond with crystalline H_2O , but it is mainly coordinated with Co^{2+} . The strength of H-bonding and the coordination of SO_4^{2-} affect the peak position of the ν_1 (SO_4) mode. The selected Raman spectra for the ν_1 (SO_4) mode shown in Fig. 14(a), (b), and (c) reveal that the wavenumbers of the bands (ν_1 (SO_4)) increased during the drying process. As the XRD analyses indicated, the changes in the ν_1 (SO_4) mode could be a consequence of the dehydration process, where 984.3, 990.3, and 1022.4 cm^{-1} correspond to heptahydrate, hexahydrate, and monohydrate, respectively. The increasing vibrational wavenumber of the ν_1 (SO_4) mode in these lower hydrates agrees with the Raman studies on various hydrates of CuSO_4 by Fu et al. (2012), CaSO_4 by Buzgar et al. (2009), and FeSO_4 by Chio et al. (2007), as shown in Table S.1.

4. Conclusions

The semi-batch vacuum evaporative crystallization of cobalt sulfate was successfully carried out in various crystallization conditions. Cobalt sulfate crystallized as monoclinic $\text{CoSO}_4 \cdot 7\text{H}_2\text{O}$, with octahedron shaped crystals at temperatures of 30 °C and 40 °C, whereas a lower hydration degree monoclinic crystal $\text{CoSO}_4 \cdot 6\text{H}_2\text{O}$ was obtained at higher temperatures of 60 °C and 80 °C. In addition, the evaporation temperature, heat energy input, and mixing speed had a significant effect on the evaporation flux, therefore affecting the particle size distribution of the products. The higher heat energy input and mixing intensity resulted in smaller crystals.

The crystallized $\text{CoSO}_4 \cdot 7\text{H}_2\text{O}$ was unstable at higher temperatures. It dehydrated easily and transformed into $\text{CoSO}_4 \cdot 6\text{H}_2\text{O}$ and $\text{CoSO}_4 \cdot \text{H}_2\text{O}$ during drying. In ambient conditions (23 °C), $\text{CoSO}_4 \cdot 7\text{H}_2\text{O}$ dehydrated and stabilized as $\text{CoSO}_4 \cdot 6\text{H}_2\text{O}$. When the drying temperature was increased to 40 °C and 60 °C, dehydration of $\text{CoSO}_4 \cdot 7\text{H}_2\text{O}$ was nearly completed to produce the monohydrate $\text{CoSO}_4 \cdot \text{H}_2\text{O}$ in stable form. Moreover, a higher drying temperature accelerated the dehydration of $\text{CoSO}_4 \cdot 7\text{H}_2\text{O}$. Based on the TG-DTA results of the crystals obtained by slow evaporative crystallization, the $\text{CoSO}_4 \cdot 7\text{H}_2\text{O}$ crystals showed to be less stable at lower dehydration temperature. Raman analysis was used to identify the hydrate forms of cobalt sulfate by comparing the vibrational wavenumber of the ν_1 (SO_4) bands. The wavenumber of ν_1 (SO_4) bands showed an increasing trend with a decrease in the degree of hydration. The combination of weight loss measurements, XRD analysis,

Raman analysis, and sample images proved to be an efficient way to study the hydrate forms and their dehydration.

The findings of the present research work provide a deeper understanding on the evaporative crystallization process of cobalt sulfate and the factors affecting the crystallized product. Evaporation at a certain underpressure and temperature range with appropriate heat energy input is a feasible way to crystallize cobalt sulfate into the desired hydrate form. Furthermore, the laboratory-scale results obtained offer a basis for achieving suitable process-scale performance.

Declaration of Competing Interest

The authors declare that they have no known competing financial interests or personal relationships that could have appeared to influence the work reported in this paper.

Acknowledgments

Zhang Jianxin wishes to acknowledge the funding from CSC (China Scholarship Council, No. 201806370220) and the Business Finland-supported BATCircle project (4853/31/2018). The authors would like to thank Chemobrionics COST Action CA17120. This work made use of Aalto University Bioeconomy and RawMatters Facilities.

Appendix A. Supplementary data

Supplementary data to this article can be found online at <https://doi.org/10.1016/j.hydromet.2022.105821>.

References

- Aktas, S., Gürcan, H., Keskin, A., Morcali, M.H., Özbey, S., Yücel, O., 2013. Investigation of cobalt sulfate precipitation by alcohol and influencing factors. *Miner. Metall. Process* 30, 174–179. <https://doi.org/10.1007/BF03402265>.
- Buzgar, N., Buzatu, A., Sanislav, I.V., 2009. The Raman study on certain sulfates. *Analele Stiintifice ale Universitatii Al. I. Cuza, Iasi, Romania* 55, 5–23. http://geology.uaic.ro/aug/articole/2009%20no1/1_L01-Buzgar%20-%20pag%205-23.pdf.
- Chio, C.H., Sharma, S.K., Muenow, D.W., 2007. The hydrates and deuterates of ferrous sulfate (FeSO_4): a Raman spectroscopic study. *J. Raman Spectrosc.* 38, 87–99. <https://doi.org/10.1002/jrs.1623>.
- Coutsouradis, D., Davin, A., Lamberigts, M., 1987. Cobalt-based superalloys for applications in gas turbines. *Mater. Sci. Eng.* 88, 11–19. [https://doi.org/10.1016/0025-5416\(87\)90061-9](https://doi.org/10.1016/0025-5416(87)90061-9).
- Devi, N.B., Nathasarma, K.C., Chakravorty, V., 1998. Separation and recovery of cobalt II and nickel II from sulphate solutions using sodium salts of D2EHFA, PC 88A and Cyanex 272. *Hydrometallurgy* 49, 47–61. [https://doi.org/10.1016/S0304-386X\(97\)00073-X](https://doi.org/10.1016/S0304-386X(97)00073-X).
- Elerman, Y., 1988. Refinement of the crystal structure of $\text{CoSO}_4 \cdot 6\text{H}_2\text{O}$. *Acta Crystallogr. C* 44, 599–601. <https://doi.org/10.1107/S0108270187012447>.
- European Commission, 2020. Study on the EU's List of Critical Raw Materials. https://rm.is.jrc.ec.europa.eu/uploads/CRM_2020_Report_Final.
- Fu, X., Yang, G., Sun, J., Zhou, J., 2012. Vibrational spectra of copper sulfate hydrates investigated with low-temperature Raman spectroscopy and terahertz time domain spectroscopy. *J. Phys. Chem. A* 116, 7314–7318. <https://doi.org/10.1021/jp302997h>.
- Giester, G., Wildner, M., 1991. The crystal structures of kieserite-type compounds. II: crystal structures of $\text{Me}(\text{II})\text{SeO}_4 \cdot \text{H}_2\text{O}$ ($\text{Me}=\text{Mg}, \text{Mn}, \text{Co}, \text{Ni}, \text{Zn}$). In: *Neues Jahrbuch Fur Mineralogie-monatshefte*, pp. 135–144.
- Huang, T., Liu, L., Zhang, S., 2019. Recovery of cobalt, lithium, and manganese from the cathode active materials of spent lithium-ion batteries in a bio-electro-hydrometallurgical process. *Hydrometallurgy* 188, 101–111. <https://doi.org/10.1016/j.hydromet.2019.06.011>.
- Li, Matthew, Lu, Jun, 2020. Cobalt in lithium-ion batteries. *Science* 367, 979–980. <https://doi.org/10.1126/science.aba9168>.
- Lide, D.R. (Ed.), 2005. *CRC Handbook of Chemistry and Physics*. CRC Press, Boca Raton, FL. Internet Version 2005.
- Lu, H., Wang, J., Wang, T., Wang, N., Bao, Y., Hao, H., 2017. Crystallization techniques in wastewater treatment: an overview of applications. *Chemosphere* 173, 474–484. <https://doi.org/10.1016/j.chemosphere.2017.01.070>.
- Mullin, J.W., 2001. *Crystallization*, Fourth ed. Butterworth-Heinemann, Oxford.
- Nandi, P.N., Kher, V.G., 1980. Thermogravimetric analysis of cobalt sulfate. *Thermochim. Acta* 41, 241–245.
- Petranikova, M., Ebin, B., Tunsu, C., 2019. Selective recovery of cobalt from the secondary streams after NiMH batteries processing using Cyanex 301. *Waste Manag.* 83, 194–201. <https://doi.org/10.1016/j.wasman.2018.11.022>.
- Rakuzin, M.A., Brodski, D.A., 1927. The dehydration of metallic salt hydrates. iv. Methods of dehydration by heat. *Z. angew. Chem* 40, 836–840.

- Reddy, B.R., Venkateswara Rao, S., Park, K.H., 2009. Solvent extraction separation and recovery of cobalt and nickel from sulphate medium using mixtures of TOPS 99 and TIBPS extractants. *Miner. Eng.* 22, 500–505. <https://doi.org/10.1016/j.mineng.2009.01.002>.
- Redhammer, G.J., Koll, L., Bernroider, M., Tippelt, G., Roth, G., 2007. Co²⁺-Cu²⁺ substitution in bieberite solid-solution series, (Co_{1-x}Cu_x)SO₄·7H₂O, 0.00 ≤ x ≤ 0.46: synthesis, single-crystal structure analysis, and optical spectroscopy. *Am. Mineral.* 92, 532–545. <https://doi.org/10.2138/am.2007.2229>.
- Said, A., Louhi-Kultanen, M., 2019. Simulation and empirical studies of solvent evaporation rates in vacuum evaporation crystallization. *Chem. Eng. Technol.* 42, 1452–1457. <https://doi.org/10.1002/ceat.201800708>.
- Sato, J., Omori, T., Oikawa, K., Ohnuma, I., Kainuma, R., Ishida, K., 2006. Cobalt-base high-temperature alloys. *Science* 312, 90–91. <https://doi.org/10.1126/science.1121738>.
- Sinha, S.G., Deshpande, N.D., Deshpande, D.A., 1989. Dehydration of crystalline CoSO₄·7H₂O. *Thermochim. Acta* 156 (1), 1–10.
- Stephen, H., Stephen, T. (Eds.), 1963. *Solubilities of Inorganic and Organic Compounds, Volume 1 Binary Systems Part 1*. Pergamon Press.
- Suslick, K.S., 1998. *Kirk-Othmer Encyclopedia of Chemical Technology*. J. Wiley & Sons, New York, p. 517, 26.
- Swain, B., Jeong, J., Lee, J. Chun, Lee, G.H., Sohn, J.S., 2007. Hydrometallurgical process for recovery of cobalt from waste cathodic active material generated during manufacturing of lithium ion batteries. *J. Power Sources* 167, 536–544. <https://doi.org/10.1016/j.jpowsour.2007.02.046>.
- Vielma, T., 2021. Thermodynamic model for CoSO₄(aq) and the related solid hydrates in the temperature range from 270 to 374 K and at atmospheric pressure. *Calphad* 72, 102230. <https://doi.org/10.1016/j.calphad.2020.102230>.
- Yang, G., Han, B., Wang, X., Yan, L., Wang, X., 2002. Synthesis of nanometer cobalt blue pigment by microemulsion. *Trans. Tianjin Univ.* 4, 16.